Multidimensional Beamspace Processing for FMCW Automotive Radar

Damir Rakhimov[*], *Ruxin Zheng*[†], *Shunqiao Sun*[†], and *Martin Haardt*[*]
[*] Communications Research Laboratory, Ilmenau University of Technology, Germany
[†] Department of Electrical and Computer Engineering, The University of Alabama, USA

***Abstract*—In this paper, we present a gridless 3-D parameter estimation method for Frequency-Modulated Continuous-Wave (FMCW) automotive radar systems that is based on the recently developed framework of 3-D ESPRIT in DFT beamspace. The proposed method is search-free and enables the simultaneous estimation of key parameters, such as azimuth, speed, and range, for every target. The algorithm incorporates a tensor representation of signals and ensures the automatic pairing of parameters across different modes. Simulation results demonstrate the effectiveness of the presented approach in achieving high-resolution parameter estimation.**

***Index Terms*—automotive radar, FMCW, harmonic retrieval, tensors, CPD, ESPRIT in DFT beamspace**

I. Introduction

Automotive radar has become an indispensable component of modern vehicles, enhancing safety and providing reliable information about the surroundings in all weather conditions [1]–[3]. Among various architectures, FMCW radar is widely adopted due to its low cost, low power consumption, and its ability to simultaneously estimate range and velocity. However, increasing demands for higher resolution require methods surpassing FFT-based periodograms, which are limited by the Rayleigh resolution limit. At the same time, advanced methods such as MUSIC [4], ESPRIT [5], and compressed sensing techniques [6], [7] overcome these limitations but are computationally impractical for automotive radars due to the constraints of the onboard processing units.

On the other hand, recent studies [8]–[10] highlight the benefits of beamspace processing, which has the potential to reduce the computational complexity by operating in a reduced-dimensional signal space and enables parallel processing for disjoint groups of beams. The beamspace transformation can be efficiently implemented via an FFT, which is a core part of the signal processing chain in modern automotive FMCW radars.

Numerous studies have explored high-resolution beamspace parameter estimation for automotive radar applications. For example, in [9], the authors propose a 1-D estimation algorithm based on beamspace MUSIC for FMCW radar to estimate the Directions of Arrival (DoAs) of impinging signals with reduced complexity when prior knowledge of the field of view is available. However, the results are limited by the use of a one-dimensional system model, which restricts applicability in multidimensional scenarios. In [11], the authors present a high-resolution algorithm for the joint estimation of range and velocity. The method employs real-valued processing and achieves pairing between the estimates via a simultaneous diagonalization of a matrix whose real and imaginary parts comprise the range and the velocity information, respectively [12]. Despite its advantages, the approach suffers from the high computational complexity of full-size element-space processing, and its pairing strategy is not applicable for multi-dimensional estimation problems. In [10], the authors present a 3-D super-resolution algorithm for millimeter wave (mmWave) FMCW radar. The method is based on a multi-dimensional extension of beamspace MUSIC, enabling the joint estimation of range, azimuth, and elevation angles. Similar to the previous study, the beamspace formulation significantly reduces the computational complexity while maintaining a high-resolution accuracy of estimates. However, despite the dimensionality reduction, the MUSIC algorithm still requires an exhaustive joint search over multiple domains, which limits its practical application. Given the limitations of the currently available methods, it is essential to investigate the alternative approaches that avoid manifold search for parameter estimation, aiming to balance computational complexity and resolution accuracy. For a comprehensive overview of the current state of research in the field of automotive radar, we refer to the review papers [1], [13], [14].

In this work, we propose a 3-D high-resolution estimation algorithm for FMCW radar, based on R-D ESPRIT in DFT beamspace [15]. The algorithm enables joint estimation of range, Doppler, and azimuth, with automatic parameter pairing across modes, achieved using Simultaneous Matrix Diagonalization (SMD) methods such as [16]. We demonstrate how the 3-D estimation method fits into the FMCW radar system model and how the target parameters can be extracted. The proposed approach belongs to the class of search-free, gridless methods while achieving a comparable estimation accuracy as the MUSIC algorithm. Additionally, the algorithm has the potential to significantly reduce the computational complexity compared to conventional methods by applying reduced-dimensional beamspace processing to the received signals when prior information is available about the Sectors of Interest (SoI).

In this paper, we follow the same notation as in [15].

The work of R. Zhang and S. Sun was supported in part by U.S. National Science Foundation (NSF) under Grants CCF-2153386 and ECCS-2340029.
The work of D. Rakhimov and M. Haardt was supported in part by the German Research Foundation (DFG) under Grant 402834619 (AdAMMM-II, HA 2239/14-3).

II. Problem Formulation

In this section, we present the signal model of an FMCW radar equipped with an array of antennas. Additional details can be found in [17]. We use the subscripts R, D, and A to denote the range, Doppler, and azimuth dimensions, respectively. For this work, we assume a single transmit antenna and M_{A} receive antennas. The receive antennas are arranged in a uniform linear array (ULA) with an equidistant spacing of $d = \lambda_{\mathrm{cr}}/2$, where λ_{cr} is the nominal carrier wavelength. Transmission consists of a sequence of M_{D} chirp pulses, where each chirp has a duration of M_{R} sampling intervals.

A. Basics of FMCW radar

The FMCW type of radar is a widely used scheme in the automotive industry due to its capability to accurately estimate the range, Doppler, and angle of detected targets. The sensing signal is transmitted in the form of a series of pulses, where an individual pulse is known as a chirp, which represents a complex-valued sinusoid with a linearly increasing instantaneous frequency over time. The instantaneous frequency of the transmitted chirp is expressed as $f_{\mathrm{T}}(t) = f_{\mathrm{cr}} + \frac{W}{T}t$, $t \in [0, T]$, where f_{cr} is the carrier frequency, W is the chirp bandwidth, and T is the pulse repetition interval (PRI) at which FMCW radars transmit chirps. For Doppler estimation, we collect a burst of M_{D} consecutive pulses. We assume that a single PRI consists of $M_{\mathrm{R}} = T/T_{\mathrm{s}}$ samples, where T_{s} is the sampling interval.

After downconversion, filtering, and sampling, the received signal for a single chirp after the environment with multiple targets can be approximated as [17]

$$z_{\mathrm{p}}(t) = \sum_{\ell=1}^{L} \alpha'_{\ell} \mathrm{exp}\left(j2\pi \left[\left(\frac{2f_{\mathrm{cr}} v_{\ell}}{\mathrm{c}} + \frac{2WR_{\ell}}{T\,\mathrm{c}} \right) t \right] \right), \quad (1)$$

where $\alpha'_{\ell} = \alpha_{\ell} \cdot \exp\left(j2\pi \frac{2f_{\mathrm{cr}} R_{\ell}}{\mathrm{c}} \right)$ is the effective intensity of the ℓ-th target and c is the speed of light.

A single chirp cannot resolve range and Doppler simultaneously, but a sequence of M_{D} chirp pulses, also known as a pulse train, can resolve these parameters. In this case, the received signal can be written as

$$z_{\mathrm{t}}(t) = \sum_{k=0}^{M_{\mathrm{D}}-1} z_{\mathrm{p}}\left(t - kT\right) \cdot \mathrm{rect}\left(\frac{t - T/2 - kT}{T} \right), \quad (2)$$

where $k \in \{0, .., M_{\mathrm{D}} - 1\}$ denotes the pulse index.

After time-domain sampling, the signal is reshaped into a matrix, where each column contains fast-time samples from a single pulse, and different columns represent slow-time snapshots across multiple pulses. The time instance of a particular sample in the pulse train is given as $t(n, k) = (n + k \cdot M_{\mathrm{R}}) \cdot T_{\mathrm{s}}$, where $n \in \{0, .., M_{\mathrm{R}} - 1\}$ represents the sample index within a chirp, M_{R} denotes the number of fast-time samples per chirp, k is the pulse index, and $T_{\mathrm{s}} \leq \frac{1}{2f_b^{\max}}$ is the sampling interval with $f_b^{\max} = \max_{\ell} \left\{ \frac{2f_c v_{\ell}}{c} + \frac{2WR_{\ell}}{T_p c} \right\}$ being the maximum beat frequency that is determined by the maximal detection range and velocity [1]. Following this convention, the signal $z_{\mathrm{t}}(t)$ can be rewritten in terms of the parameters n and k as

$$z_{\mathrm{t}}(n, k) = \sum_{\ell=1}^{L} \alpha'_{\ell} \mathrm{exp}\left(j\, n\, \mu_{\mathrm{R},\ell} + j\, k\, \mu_{\mathrm{D},\ell} \right), \quad (3)$$

where $\mu_{\mathrm{R},\ell} = 2\pi \left(\frac{2f_{\mathrm{cr}} v_{\ell}}{\mathrm{c}} + \frac{2WR_{\ell}}{T\mathrm{c}} \right) T_{\mathrm{s}}$ is the angular frequency for range, and $\mu_{\mathrm{D},\ell} = 2\pi \frac{2f_{\mathrm{cr}} v_{\ell}}{\mathrm{c}} M_{\mathrm{R}} T_{\mathrm{s}}$ is the angular frequency for velocity, where we have imposed an additional assumption, $\frac{2WR_{\ell}}{T\mathrm{c}} M_{\mathrm{R}} T_{\mathrm{s}} \approx 0$ to simplify the resulting expression.

B. Signal Model for a Uniform Linear Array

For a ULA, depending on the index of the antenna element, the received signal will experience an additional delay, which depends on the direction of arrival. Assuming the first antenna element as a reference point and far-field propagation, the delay at the m-th antenna element can be expressed as $\tau_{\mathrm{A},\ell}[m] = m \frac{d}{\mathrm{c}} \sin(\theta_{\ell})$, where $m \in \{0, .., M_{\mathrm{A}} - 1\}$ is the antenna index, d is the spacing between adjacent antenna elements, and θ_{ℓ} is the angle of arrival of the ℓ-th source with respect to the boresight direction.

Assuming a narrowband model, the signal at the m-th antenna can be rewritten as

$$s(t - \tau_{\mathrm{A},\ell}[m]) \approx s(t) \mathrm{exp}\left(-j2\pi f_{\mathrm{cr}} \tau_{\mathrm{A},\ell}[m] \right) = s(t) \mathrm{e}^{j\, m\, \mu_{\mathrm{A},\ell}}, \quad (4)$$

where $\mu_{\mathrm{A},\ell} = -2\pi \frac{d}{\lambda_{\mathrm{cr}}} \sin(\theta_{\ell})$ is the spatial frequency corresponding to the azimuth of the ℓ-th target.

C. Tensor Signal Model

The noiseless received signal after downconversion $z_{\mathrm{t}}(t)$ at the m-th antenna for the n-th sample of the k-th chirp pulse can be written as

$$z_{\mathrm{t}}(m, n, k) = \sum_{\ell=1}^{L} \alpha'_{\ell} \mathrm{e}^{jn\mu_{\mathrm{R},\ell} + jk\mu_{\mathrm{D},\ell} + jm\mu_{\mathrm{A},\ell}}. \quad (5)$$

Hence, the overall received signal, collected from M_{A} antennas over M_{D} chirp pulses, with each chirp containing M_{R} samples, can be represented as a tensor $\boldsymbol{\mathcal{Z}} \in \mathbb{C}^{M_{\mathrm{R}} \times M_{\mathrm{D}} \times M_{\mathrm{A}}}$. This tensor can be written in a compact form via a Canonical Polyadic Decomposition (CPD) [18] as

$$\boldsymbol{\mathcal{Z}} = \boldsymbol{\mathcal{I}}_{4,L} \times_1 \boldsymbol{A}_{\mathrm{R}} \times_2 \boldsymbol{A}_{\mathrm{D}} \times_3 \boldsymbol{A}_{\mathrm{A}} \times_4 \boldsymbol{\alpha}^{\mathrm{T}}, \quad (6)$$

where $\boldsymbol{A}_r \in \mathbb{C}^{M_r \times L}$, $\forall r \in \{\mathrm{R}, \mathrm{D}, \mathrm{A}\}$ is the Vandermonde matrix with the ℓ-th column defined as $\boldsymbol{a}_{r,\ell} = \left[1,\ \mathrm{e}^{j\mu_{r,\ell}}, \cdots, \mathrm{e}^{j(M_r - 1)\mu_{r,\ell}} \right]^{\mathrm{T}}$ and $\boldsymbol{\alpha} = \left[\alpha'_1, \cdots, \alpha'_L \right]^{\mathrm{T}}$ is the vector with intensity coefficients for all targets.

The obtained system representation is a canonical signal model for multidimensional high-resolution parameter estimation (HRPE). Thus, the corresponding frequencies can be estimated via various available state-of-the-art algorithms for multidimensional parameter estimation, such as [15].

D. Additional Preprocessing Steps

In highly dynamic environments with limited snapshots and correlated echoes, subspace-based methods may fail to provide accurate estimates of target parameters. In such scenarios,

preprocessing techniques such as Spatial Smoothing (SpS) and Forward-Backward Averaging (FBA) might help decorrelate signals and increase the number of available samples for subspace estimation [19], [20].

In this work, despite having a limited number of antennas and chirp pulses, SpS is applied along each dimension. The simulation results show that this leads to improved parameter estimation accuracy across all modes.

E. Beamspace Transformation

Let $\boldsymbol{F}_r \in \mathbb{C}^{M_r \times M_r}, \forall r \in \{\mathrm{R}, \mathrm{D}, \mathrm{A}\}$ be the DFT beamspace transformation matrix for the r-th mode with phase-shifted and normalized columns. The κ_r-th column related to the beam $\kappa_r \in \{0, .., M_r - 1\}$ can be written as

$$\boldsymbol{f}_{\kappa_r}^{(r)} = \frac{\mathrm{e}^{-j\left(\frac{M_r-1}{2}\right)\gamma_{\kappa_r}}}{\sqrt{M_r}} \begin{bmatrix} 1 & \mathrm{e}^{j\gamma_{\kappa_r}} & \cdots & \mathrm{e}^{j\left(M_r-1\right)\gamma_{\kappa_r}} \end{bmatrix}^{\mathrm{T}}, \quad (7)$$

where $\gamma_{\kappa_r} = \kappa_r \frac{2\pi}{M_r}$ is the center of the κ_r-th beam, $\forall r \in \{\mathrm{R}, \mathrm{D}, \mathrm{A}\}$. Please note that the matrix $\boldsymbol{F}_r$ can be obtained by applying an FFT transform followed by a multiplication with a diagonal matrix containing the corresponding phase shifts.

The signal $\boldsymbol{\mathcal{Z}}_{\mathrm{dft}} \in \mathbb{C}^{M_\mathrm{R} \times M_\mathrm{D} \times M_\mathrm{A} \times 1}$ after the beamspace transformation can be written in a tensor form as

$$\begin{aligned} \boldsymbol{\mathcal{Z}}_{\mathrm{dft}} &= \boldsymbol{\mathcal{Z}} \times_1 \boldsymbol{F}_\mathrm{R}{}^\mathrm{H} \times_2 \boldsymbol{F}_\mathrm{D}{}^\mathrm{H} \times_3 \boldsymbol{F}_\mathrm{A}{}^\mathrm{H} \\ &= \underbrace{\boldsymbol{\mathcal{I}}_{4,L} \times_1 \boldsymbol{B}_\mathrm{R} \times_2 \boldsymbol{B}_\mathrm{D} \times_3 \boldsymbol{B}_\mathrm{A}}_{\boldsymbol{\mathcal{B}}} \times_4 \boldsymbol{\alpha}^\mathrm{T}, \end{aligned} \quad (8)$$

where the matrix $\boldsymbol{B}_r = \boldsymbol{F}_r{}^\mathrm{H} \cdot \boldsymbol{A}_r \in \mathbb{C}^{M_r \times L}, \forall r \in \{\mathrm{R}, \mathrm{D}, \mathrm{A}\}$ is the beamspace steering matrix for the r-th mode and the tensor $\boldsymbol{\mathcal{B}} \in \mathbb{C}^{M_\mathrm{R} \times M_\mathrm{D} \times M_\mathrm{A}}$ is the DFT beamspace steering tensor for all modes.

Algorithm 1 3-D ESPRIT in DFT Beamspace for automotive FMCW radar

1: **Training phase**
- Collect received signals for M_D chirp pulses
- Build the received signal tensor $\boldsymbol{\mathcal{Z}} \in \mathbb{C}^{M_\mathrm{R} \times M_\mathrm{D} \times M_\mathrm{A} \times 1}$

2: **Pre-processing**
- Perform Smoothing along each mode
  - $\boldsymbol{\mathcal{Z}}_{\mathrm{sps}} \in \mathbb{C}^{M_{\mathrm{sub,R}} \times M_{\mathrm{sub,D}} \times M_{\mathrm{sub,A}} \times N_{\mathrm{sub}}}$
- Calculate beamspace transformation along each mode
  - $\boldsymbol{\mathcal{Z}}_{\mathrm{dft}} = \boldsymbol{\mathcal{Z}}_{\mathrm{sps}} \times_1 \boldsymbol{F}_\mathrm{R}{}^\mathrm{H} \times_2 \boldsymbol{F}_\mathrm{D}{}^\mathrm{H} \times_3 \boldsymbol{F}_\mathrm{A}{}^\mathrm{H}$
- Apply Forward-Backward averaging
  - $\boldsymbol{\mathcal{Z}}_{\mathrm{fba}} = \sqrt{2} \left[\boldsymbol{\mathcal{Z}}_{\mathrm{dft}} \hookrightarrow_4 \boldsymbol{\mathcal{Z}}^*_{\mathrm{dft}} \right]$

3: **Signal subspace estimation**
- Compute SVD of $\left[\boldsymbol{\mathcal{Z}}_{\mathrm{fba}} \right]^\mathrm{T}_{(4)}$ and truncate it to rank L
  - $\left[\boldsymbol{\mathcal{Z}}_{\mathrm{fba}} \right]^\mathrm{T}_{(4)} \approx \boldsymbol{U}_\mathrm{s} \cdot \boldsymbol{\Sigma}_\mathrm{s} \cdot \boldsymbol{V}_\mathrm{s}^\mathrm{H}$
- Determine the signal subspace tensor $\boldsymbol{\mathcal{U}}_\mathrm{s}$
  - $\boldsymbol{\mathcal{U}}_\mathrm{s} = \text{reshape}\left\{\boldsymbol{U}_\mathrm{s}\right\} \in \mathbb{C}^{M_{\mathrm{sub,R}} \times M_{\mathrm{sub,D}} \times M_{\mathrm{sub,A}} \times L}$

4: **Solution of the shift-invariance equations**
- Construct the beamspace selection matrices for each mode
  - $\boldsymbol{G}_{r,1} \in \mathbb{C}^{M_r \times M_r}$ and $\boldsymbol{G}_{r,2} \in \mathbb{C}^{M_r \times M_r}, \forall r \in \{\mathrm{R}, \mathrm{D}, \mathrm{A}\}$
- Construct 3 shift invariance equations
  - $\boldsymbol{\mathcal{U}}_\mathrm{s} \times_r \boldsymbol{G}_{r,1} \times_4 \boldsymbol{\Psi}_r \approx \boldsymbol{\mathcal{U}}_\mathrm{s} \times_r \boldsymbol{G}_{r,2}, \forall r \in \{\mathrm{R}, \mathrm{D}, \mathrm{A}\}$
- Solve the equations for $\boldsymbol{\Psi}_r \in \mathbb{C}^{L \times L}, \forall r$, e.g., via LS

5: **Angular frequency estimation**
- Obtain the estimates of $\hat{\boldsymbol{\Phi}}_r$ via joint EVD of $\boldsymbol{\Psi}_r, \forall r$
- Compute estimates of frequencies
  - $\hat{\mu}_{r,\ell} = \arg\left(\lambda_{r,\ell}\right), \forall r \in \{\mathrm{R}, \mathrm{D}, \mathrm{A}\}, \forall \ell \in \{1, .., L\}$

6: **Target parameters estimation**
- Calculate velocity as $v_\ell = \frac{\hat{\mu}_{\mathrm{D},\ell} c}{4\pi f_{\mathrm{cr}} T_\mathrm{s}}, \forall \ell$
- Calculate range as $R_\ell = \left(\frac{\hat{\mu}_{\mathrm{R},\ell}}{2\pi T_\mathrm{s}} - \frac{2 f_{\mathrm{cr}} v_\ell}{\mathrm{c}}\right) \frac{T\mathrm{c}}{2W}, \forall \ell$
- Calculate angle as $\theta_\ell = \arcsin\left(-\frac{\hat{\mu}_{\mathrm{A},\ell} \lambda_{\mathrm{cr}}}{2\pi d}\right), \forall \ell$

III. 3-D ESPRIT IN DFT BEAMSPACE

This section provides a short summary of 3-D ESPRIT in DFT Beamspace for a noiseless signal model.

Following [12], [15], we can write a shift-invariance equation for L targets impinging the sensor grid in the r-th mode and the full-size DFT beamspace transformation as

$$\boldsymbol{G}_{r,1} \boldsymbol{B}_r \boldsymbol{\Phi}_r = \boldsymbol{G}_{r,2} \boldsymbol{B}_r \in \mathbb{C}^{M_r \times L}, \quad (9)$$

where $\boldsymbol{\Phi}_r = \mathrm{diag}\left(\mathrm{e}^{j\mu_{r,\ell}}\right)_{\ell=1}^{L}$ is a diagonal matrix with information about the spatial directions towards different targets in the r-th mode, $\boldsymbol{G}_{r,1} \in \mathbb{C}^{M_r \times M_r}$ and $\boldsymbol{G}_{r,2} \in \mathbb{C}^{M_r \times M_r}$ are the selection matrices[1] defined as

$$\boldsymbol{G}_{r,1} = \begin{bmatrix} 1 & \mathrm{e}^{-j\frac{\pi}{M_r}} & 0 & \cdots & 0 \\ 0 & \mathrm{e}^{-j\frac{\pi}{M_r}} & \mathrm{e}^{-j\frac{2\pi}{M_r}} & \cdots & 0 \\ 0 & 0 & \mathrm{e}^{-j\frac{2\pi}{M_r}} & \cdots & 0 \\ \vdots & \vdots & \vdots & \ddots & \vdots \\ (-1)^{M_r} & 0 & 0 & \cdots & \mathrm{e}^{-j(M_r-1)\frac{\pi}{M_r}} \end{bmatrix} \quad (10)$$

and $\boldsymbol{G}_{r,2} = \boldsymbol{G}^*_{r,1}$.

This shift-invariance property can also be written in the tensor form as

$$\boldsymbol{\mathcal{B}} \times_r \boldsymbol{G}_{r,1} \times_4 \boldsymbol{\Phi}_r = \boldsymbol{\mathcal{B}} \times_r \boldsymbol{G}_{r,2}, \quad (11)$$

[1]Please note that the full-size selection matrices $\boldsymbol{G}_{r,1}$ and $\boldsymbol{G}_{r,2}$ are only of rank $(M-1)$. Therefore, one of the M rows can be excluded in case of processing in full-dimensional DFT beamspace.

where $\boldsymbol{\mathcal{B}} \in \mathbb{C}^{M_\mathrm{R} \times M_\mathrm{D} \times M_\mathrm{A}}$ is the beamspace steering tensor for all modes. The matrix $\boldsymbol{\Phi}_r = \mathrm{diag}\left(\mathrm{e}^{j\mu_{r,\ell}}\right)_{\ell=1}^{L} \in \mathbb{C}^{L \times L}$ contains the information about the spatial directions towards different sources in the r-th mode.

The shift-invariance property for the r-th mode can also be written in a matrix form via the 4-mode unfolding of the beamspace steering tensor as

$$\tilde{\boldsymbol{G}}_{r,1} \cdot \left[\boldsymbol{\mathcal{B}}\right]^\mathrm{T}_{(4)} \cdot \boldsymbol{\Phi}_r = \tilde{\boldsymbol{G}}_{r,2} \cdot \left[\boldsymbol{\mathcal{B}}\right]^\mathrm{T}_{(4)}, \quad (12)$$

where $\tilde{\boldsymbol{G}}_{r,j} \in \mathbb{C}^{M \times M}, j \in \{1, 2\}$, $M = \prod_{r=1}^{3} M_r$ is the matrix version of the multidimensional selection matrices that can be found as

$$\tilde{\boldsymbol{G}}_{r,j} = \boldsymbol{I}_{\prod_{\bar{r}=r+1}^{3} M_{\bar{r}}} \otimes \boldsymbol{G}_{r,j} \otimes \boldsymbol{I}_{\prod_{\bar{r}=1}^{r-1} M_{\bar{r}}}. \quad (13)$$

During the estimation step, the tensor $\boldsymbol{\mathcal{B}} \in \mathbb{C}^{M_\mathrm{R} \times M_\mathrm{D} \times M_\mathrm{A} \times L}$ is unknown, but we can calculate the corresponding tensor signal subspace $\boldsymbol{\mathcal{U}}_\mathrm{s}$ via an SVD that is related to the steering tensor as $\boldsymbol{\mathcal{B}} = \boldsymbol{\mathcal{U}}_\mathrm{s} \times_4 \boldsymbol{K}$. Hence, we rewrite equation (12) by

$$\tilde{\boldsymbol{G}}_{r,1} \left[\boldsymbol{\mathcal{U}}_\mathrm{s}\right]^\mathrm{T}_{(4)} \underbrace{\boldsymbol{K} \boldsymbol{\Phi}_r \boldsymbol{K}^{-1}}_{\boldsymbol{\Psi}_r} = \tilde{\boldsymbol{G}}_{r,2} \left[\boldsymbol{\mathcal{U}}_\mathrm{s}\right]^\mathrm{T}_{(4)}. \quad (14)$$

In the next step, we estimate the matrix $\boldsymbol{\Psi}_r$ using, for example, the method of least squares as

$$\boldsymbol{\Psi}_r = \left(\tilde{\boldsymbol{G}}_{r,1} \left[\boldsymbol{\mathcal{U}}_\mathrm{s}\right]^\mathrm{T}_{(4)}\right)^{+} \cdot \left(\tilde{\boldsymbol{G}}_{r,2} \left[\boldsymbol{\mathcal{U}}_\mathrm{s}\right]^\mathrm{T}_{(4)}\right). \quad (15)$$

Then the matrix $\boldsymbol{\Phi}_r$ can be estimated via an eigenvalue decomposition of $\boldsymbol{\Psi}_r$ since $\boldsymbol{\Phi}_r$ is diagonal and the product $\boldsymbol{K}\boldsymbol{\Phi}_r\boldsymbol{K}^{-1}$ has a similar form as an eigenvalue decomposition. To achieve automatic pairing between the parameters in different modes, a joint eigenvalue decomposition or Schur decomposition can be calculated to diagonalize the matrices $\boldsymbol{\Phi}_r$ simultaneously for all modes and find the eigenvalues $\boldsymbol{\Lambda}_r = \boldsymbol{Q}\,\boldsymbol{\Psi}_r\,\boldsymbol{Q}^{-1}$, $\forall r \in \{\mathrm{R},\mathrm{D},\mathrm{A}\}$, where $\boldsymbol{Q}$ is a matrix with the common eigenvectors for all modes.

Finally, we compute the estimates of the spatial frequencies $\hat{\mu}_{r,\ell}$ by taking the arguments of the estimated eigenvalues, i.e., $\hat{\mu}_{r,\ell} = \arg\left(\lambda_{r,\ell}\right)$, $\forall r \in \{\mathrm{R},\mathrm{D},\mathrm{A}\}, \forall \ell \in \{1,..,L\}$.

A. Complexity Analysis

The computational complexity of the proposed algorithm is summarized in Table 1. Here, $M_{\mathrm{sub}} = \prod_{r=1}^{\{\mathrm{R},\mathrm{D},\mathrm{A}\}} M_{\mathrm{sub},r}$ is the total number of effective sensors and $2N_{\mathrm{sub}}$ is the the resulting number of snapshots after applying spatial smoothing and forward-backward averaging across all three dimensions. The number of targets to estimate is denotes as L.

Operation	Complexity
Beamspace Transformation	$\mathcal{O}\left\{2N_{\mathrm{sub}}M_{\mathrm{sub}}\log_2\left(M_{\mathrm{sub}}\right)\right\}$
Signal subspace estimation	$\mathcal{O}\left\{4M_{\mathrm{sub}}N_{\mathrm{sub}}^2\right\}$
Shift-invariance equation	$\mathcal{O}\left\{M_{\mathrm{sub}}L^2\right\}$
Frequency Estimation & Pairing	$\mathcal{O}\left\{3L^3\right\}$

Table 1: Complexity Analysis

IV. Simulation results

In this section, we present selected simulation results to demonstrate the performance of the proposed algorithm.

We compare the proposed method with the conventional FFT-based method for parameter estimation [1]. It selects L beams with the highest magnitudes in one dimension at a time.

For the simulation setup, we consider the following system configuration. Each chirp pulse consists of $M_{\mathrm{R}} = 64$ samples for range estimation, and the pulse train contains $M_{\mathrm{D}} = 32$ pulses. The receiver antenna array is equipped with $M_{\mathrm{A}} = 16$ antennas. The signal chirp is generated using the expression given in (1). For the preprocessing stage of the ESPRIT-type algorithm, we apply spatial smoothing, forward-backward averaging, and a full-size DFT beamspace transformation. We assume the received signal is corrupted by an Additive Zero-Mean Circularly Symmetrical Complex Gaussian (ZMCSCG) noise with variance σ_n^2. The signal-to-noise-ratio (SNR) is defined as $\mathrm{SNR} = 10\log\frac{\sum_\ell^L \alpha_\ell^2}{\sigma_n^2}$, where α_ℓ represents the intensity of the ℓ-th target. All simulation results presented in Figure 1 are obtained through Monte Carlo trials, where each point is averaged over $1,000$ realizations of ZMCSCG noise.

In the simulation results, 3-D ESPRIT in DFT beamspace is labeled as (`SBE`), with additional information about the configuration for smoothing in parentheses. The FFT-based approach is denoted as (`DFT`), where the coefficient in the parentheses after the label specifies the oversampling factor. For comparison purposes, we also include the deterministic Cramér-Rao Lower Bound (CRLB) for (6) in the figures with the other simulation results. It is depicted as a black dashed line with the label (`Det CRLB`) and is calculated similarly to the approach described in [21].

To make the comparison of simulation results across different modes consistent, we measure the performance of each algorithm using the Root Mean Squared Error (RMSE) of the corresponding angular frequencies in each mode. The RMSE for the r-th mode is given by the expression

$$\mathrm{RMSE}_r = \sqrt{\mathbb{E}\left\{\frac{1}{L}\sum_{\ell=1}^{L}\left(\hat{\mu}_{r,\ell}-\mu_{r,\ell}\right)^2\right\}}, \forall r \in \{\mathrm{R},\mathrm{D},\mathrm{A}\}. \quad (16)$$

The main parameters of the simulated environment, such as range, velocity, azimuth, and intensity, are listed in Table 2.

Target	$R_\ell, [\mathrm{m}]$	$v_\ell, [\mathrm{m/s}]$	$\theta_\ell, [^\circ]$	α_ℓ
1	5	3	50	1
2	12	-10	20	0.85
3	20	27	-20	0.7
4	15	35	5	0.5

Table 2: Simulation parameters

Figure 1(a) shows the total RMSE across all dimensions. We can observe that the error for `SBE` continues to decrease as the SNR increases, while the `DFT` method reaches a plateau beyond a certain SNR level due to its inherent resolution limit. Furthermore, it can be observed that different configurations of smoothing result in varying estimation accuracy. The configuration with $N_{\mathrm{sub}} = \{\ 17\times 9\times 5\ \}$ subarrays leads to the best performance, especially for the low SNR range. This indicates a trade-off between the effective aperture size after smoothing and the resulting number of available snapshots. The underlying mechanism behind this trade-off can be further investigated through an analytical assessment of the algorithm in future work. Figures 1(b), 1(c), and 1(d) present the RMSE versus SNR for each dimension individually. It can be observed in Figure 1(d) that the `DFT` method outperforms `SBE` in a certain SNR range, which happens due to the usage of a specific implementation and its sequential processing across dimensions, which progressively reduces the search space and accumulates additional gain for the remaining dimensions.

In general, based on the presented simulation results, we can confirm the ability of the proposed algorithm to provide high-resolution estimates of target parameters with accuracy exceeding the Rayleigh resolution limit.

V. Conclusions

In this paper, we present a gridless 3-D parameter estimation method for FMCW automotive radar systems based on the framework of 3-D ESPRIT in DFT beamspace. The proposed algorithm enables the simultaneous estimation of target parameters, including azimuth, speed, and range, while ensuring automatic pairing of parameters across different modes. Simulation results confirm the capability of the proposed algorithm to achieve high-resolution estimates of target parameters. For future work, the approach can be extended to MIMO radar systems and combined with reduced-dimensional processing to decrease the computational complexity.

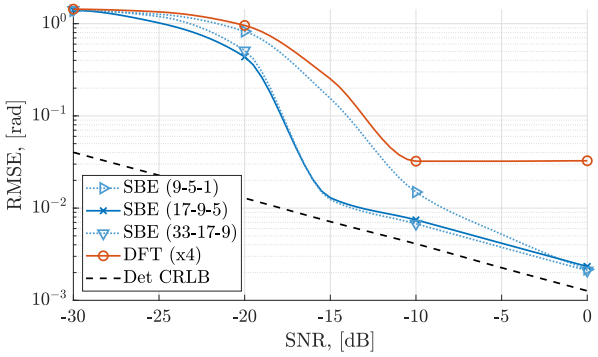

(a) Total RMSE versus SNR for all dimensions.

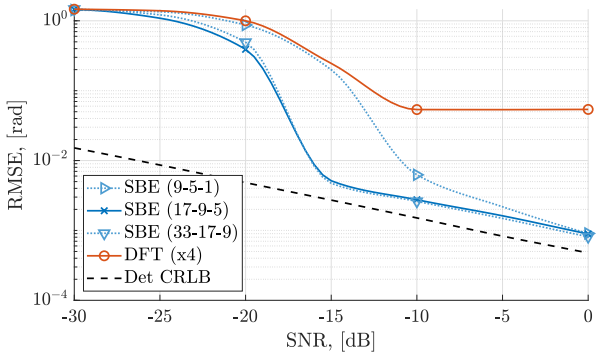

(b) $\mathrm{RMSE_R}$ versus SNR for the range dimension.

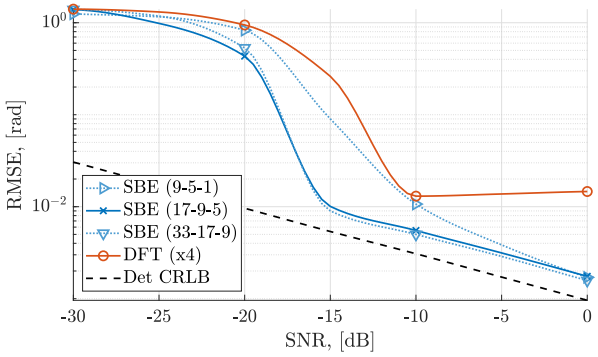

(c) $\mathrm{RMSE_D}$ versus SNR for the Doppler dimension.

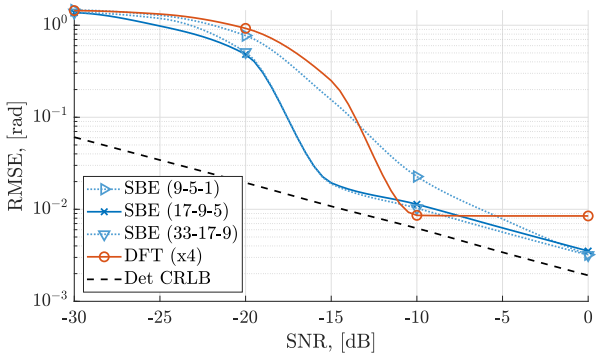

(d) $\mathrm{RMSE_A}$ versus SNR for the azimuth dimension.

Figure 1: Simulation results for Automotive radar based on 3-D ESPRIT in DFT beamspace.

REFERENCES

[1] S. Sun, A. P. Petropulu, and H. V. Poor, "MIMO radar for Advanced driver-assistance systems and autonomous driving: Advantages and challenges," *IEEE Signal Processing Magazine*, vol. 37, no. 4, pp. 98–117, Jul. 2020.

[2] S. Sun and Y. D. Zhang, "4D automotive radar sensing for autonomous vehicles: A sparsity-oriented approach," *IEEE Journal of Selected Topics in Signal Processing*, vol. 15, no. 4, pp. 879–891, Jun. 2021.

[3] R. Zheng, S. Sun, H. Liu, and T. Wu, "Deep neural networks-enabled vehicle detection using high-resolution automotive radar imaging," *IEEE Transactions on Aerospace and Electronic Systems*, vol. 59, no. 5, pp. 4815–4830, May 2023.

[4] R. Schmidt, "Multiple emitter location and signal parameter estimation," *IEEE Transactions on Antennas and Propagation*, vol. 34, no. 3, pp. 276–280, Mar. 1986.

[5] R. Roy, A. Paulraj, and T. Kailath, "ESPRIT – A subspace rotation approach to estimation of parameters of cisoids in noise," *IEEE Transactions on Acoustics, Speech, and Signal Processing*, vol. 34, no. 5, pp. 1340–1342, Oct. 1986.

[6] J. A. Tropp and A. C. Gilbert, "Signal Recovery From Random Measurements Via Orthogonal Matching Pursuit," *IEEE Transactions on Information Theory*, vol. 53, no. 12, pp. 4655–4666, Dec. 2007.

[7] T. Yardibi, J. Li, P. Stoica, M. Xue, and A. B. Baggeroer, "Source Localization and Sensing: A Nonparametric Iterative Adaptive Approach Based on Weighted Least Squares," *IEEE Transactions on Aerospace and Electronic Systems*, vol. 46, no. 1, pp. 425–443, Jan. 2010.

[8] D. Rakhimov, J. Zhang, A. L. F. Almeida, A. Nadeev, and M. Haardt, "Channel Estimation for Hybrid Multi-Carrier mmWave MIMO Systems Using 3-D Unitary Tensor-ESPRIT in DFT beamspace," in *Proc. 53rd Asilomar Conference on Signals, Systems, and Computers*, Pacific Grove, CA, USA, Oct. 2019, pp. 447–451.

[9] Y. Li, C. Zhang, Y. Song, and Y. Huang, "Enhanced beamspace MUSIC for cost-effective FMCW automotive radar," *IET Radar, Sonar & Navigation*, vol. 14, no. 2, pp. 257–267, Feb. 2020.

[10] S. Patole, A. B. Baral, and M. Torlak, "Fast 3D Joint Superresolution Algorithm for Millimeter Wave FMCW Radars," *IEEE Open Journal of Signal Processing*, vol. 4, pp. 346–365, Jun. 2023.

[11] D. Wen, H. Yi, W. Zhang, and H. Xu, "2D-Unitary ESPRIT Based Multi-Target Joint Range and Velocity Estimation Algorithm for FMCW Radar," *Applied Sciences*, vol. 13, no. 18, pp. 1–16, Jan. 2023.

[12] M. D. Zoltowski, M. Haardt, and C. P. Mathews, "Closed-form 2-D angle estimation with rectangular arrays in element space or beamspace via unitary ESPRIT," *IEEE Transactions on Signal Processing*, vol. 44, no. 2, pp. 316–328, Feb. 1996.

[13] S. M. Patole, M. Torlak, D. Wang, and M. Ali, "Automotive radars: A review of signal processing techniques," *IEEE Signal Processing Magazine*, vol. 34, no. 2, pp. 22–35, Mar. 2017.

[14] G. Hakobyan and B. Yang, "High-Performance Automotive Radar: A Review of Signal Processing Algorithms and Modulation Schemes," *IEEE Signal Processing Magazine*, vol. 36, no. 5, pp. 32–44, Sep. 2019.

[15] J. Zhang, D. Rakhimov, and M. Haardt, "Gridless Channel Estimation for Hybrid mmWave MIMO Systems via Tensor-ESPRIT Algorithms in DFT Beamspace," *IEEE Journal of Selected Topics in Signal Processing*, vol. 15, no. 3, pp. 816–831, Mar. 2021.

[16] T. Fu and X. Gao, "Simultaneous diagonalization with similarity transformation for non-defective matrices," in *Proc. IEEE International Conference on Acoustics Speech and Signal Processing (ICASSP 2006)*, vol. 4, Toulouse, France, May 2006, pp. 1137–1140.

[17] A. Stove, "Linear FMCW radar techniques," *IEE Proceedings F (Radar and Signal Processing)*, vol. 139, no. 5, pp. 343–350, Oct. 1992.

[18] T. G. Kolda and B. W. Bader, "Tensor Decompositions and Applications," *SIAM Review*, vol. 51, no. 3, pp. 455–500, Aug. 2009.

[19] T.-J. Shan, M. Wax, and T. Kailath, "On spatial smoothing for direction-of-arrival estimation of coherent signals," *IEEE Transactions on Acoustics, Speech, and Signal Processing*, vol. 33, no. 4, pp. 806–811, Aug. 1985.

[20] S. Pillai and B. Kwon, "Forward/backward spatial smoothing techniques for coherent signal identification," *IEEE Transactions on Acoustics, Speech, and Signal Processing*, vol. 37, no. 1, pp. 8–15, Jan. 1989.

[21] D. Rakhimov, A. Rakhimov, A. Nadeev, and M. Haardt, "Tensor Formulation of the Cramer-Rao Lower Bound for Beamspace Channel Estimation in mmWave MIMO-OFDM," in *Proc. 25th International ITG Workshop on Smart Antennas (WSA 2021)*, Nice, France, Nov. 2021, pp. 29–34.